Absolute quantum yield measurements for the formation of oxygen atoms after UV laser excitation of SO₂ at 222·4 nm

MOHAMMED ABU-BAJEH[a], MELANIE CAMERON[b],
KYUNG-HOON JUNG[c], CHRISTOPH KAPPEL[d], ALMUTH LÄUTER[a],
KYOUNG-SEOK LEE[c], HARI P UPADHYAYA[e], RAJESH K VATSA[e] and
HANS-ROBERT VOLPP[a]*

[a]Physikalisch-Chemisches Institut der Universität Heidelberg, Im
Neuenheimer Feld 253, D-69120 Heidelberg, Germany
[b]Max-Planck-Institut für Chemie, Division of Atmospheric Chemistry,
D-55020 Mainz, Germany
[c]Department of Chemistry and Molecular Science Institute (BK21), Korea
Advanced Institute of Science and Technology (KAIST), Yusung-Gu,
Taejon 305-701, Korea
[d]Institut für Physikalische Chemie der Universität Göttingen, D-37075
Göttingen, Germany
[e]Chemistry and Isotope Group, Bhabha Atomic Research Center,
Mumbai 400 085, India
e-mail: aw2@ix.urz.uni-heidelberg.de

Abstract. The dynamics of formation of oxygen atoms after UV photoexcitation of SO₂ in the gas-phase was studied by pulsed laser photolysis-laser-induced fluorescence 'pump-and-probe' technique in a flow reactor. SO₂ at room-temperature was excited at the KrCl excimer laser wavelength (222·4 nm) and $O(^3P_j)$ photofragments were detected under collision-free conditions by vacuum ultraviolet laser-induced fluorescence. The use of narrow-band probe laser radiation, generated via resonant third-order sum-difference frequency conversion of dye laser radiation in Krypton, allowed the measurement of the nascent $O(^3P_{j=2,1,0})$ fine-structure state distribution: $n_{j=2}/n_{j=1}/n_{j=0} = (0.88 \pm 0.02)/(0.10 \pm 0.01)/(0.02 \pm 0.01)$. Employing NO₂ photolysis as a reference, a value of $\Phi_{O(^3P)} = 0.13 \pm 0.05$ for the absolute $O(^3P)$ atom quantum yield was determined. The measured $O(^3P)$ quantum yield is compared with the results of earlier fluorescence quantum yield measurements. A suitable mechanism is suggested in which the dissociation proceeds via internal conversion from high rotational states of the initially excited $SO_2(\tilde{C}\,^1B_2)$ (1, 2, 2) vibronic level to nearby continuum states of the electronic ground state.

Keywords. Sulphur dioxide; photodissociation dynamics; oxygen atom; VUV-LIF; quantum yield.

1. Introduction

Direct emission of sulphur dioxide, SO₂, from anthropogenic activities such as coal combustion in power plants, is the largest individual source of sulphur in the earth's troposphere.[1] Due to its importance as a combustion and atmospheric trace species the thermal decomposition kinetics and photochemistry of SO₂ have been studied for many

---

*For correspondence

years.[2,3] Earlier spectroscopic and photochemical results obtained in the wavelength region 105–390 nm were reviewed in great detail by Okabe.[4] Most recent work has focused on the high-resolution spectroscopic characterisation of the SO_2 vibronic bands in the wavelength range 292–329 nm and the state-resolved dissociation dynamics of SO_2 following laser photoexcitation in the structured electronic absorption band in the 180–235 nm region.[5,6] The latter band has been assigned to an optical transition from the $\tilde{X}\,^1A_1$ ground state of SO_2 to the third excited singlet state, $\tilde{C}\,^1B_2$, located 42573 cm^{-1} above the ground state.[7] which can lead to the formation of $SO(X^3\Sigma^-)$ and $O(^3P)$ photofragments via a predissociation mechanism.[8]

A number of studies have been carried out in which the products from the SO_2 dissociation after photoexcitation at the ArF excimer laser wavelength (193·3 nm) were detected employing different spectroscopic methods.[9–18] The first study of the dynamics of this process was carried out by Freedman *et al*, who applied the molecular beam photofragment time-of-flight (TOF) technique to determine the translational energy distribution of the SO fragments.[9] Based on their measured translational energy distribution they concluded that the majority of the SO products should be produced in the $v'' = 3$ and $v'' = 4$ vibrational states. These experiments were later repeated by Kawasaki *et al*[10] with a pulsed molecular beam source. In these experiments the angular distribution of the SO fragments was measured and found to be isotropic. In a subsequent study Kawasaki *et al*[11] measured the O atom TOF distribution from which they derived a SO vibrational state distribution with a maximum at $v'' = 2$. In a reinvestigation of the SO product translational energy release with a high-resolution molecular beam photofragment TOF apparatus, Felder *et al*[12,13] obtained a SO vibrational state distribution which was found to be in good agreement with the distribution measured by Kanamori *et al* in the gas-phase photodissociation study using diode laser spectroscopy for SO detection.[14] The latter SO vibrational distributions, however, were found to be more sharply peaked at $v'' = 2$ than the earlier one reported in ref. [11]. Experiments in which $SO(X^3\Sigma^-)$ products were detected by laser-induced fluorescence (LIF) and molecular beam-Fourier transform microwave spectroscopy were reported in refs. [15] and [16] respectively. So far two gas-phase photolysis studies of SO_2 at 193·3 nm have been reported in which dynamics of the formation of $O(^3P)$ atom was investigated by LIF spectroscopy.[17,18] However, markedly different $O(+3P_j = 2, 1, 0)$ fine-structure state distributions were obtained in the latter studies which do not agree within their uncertainty limits.

Several experiments were performed to investigate the fragmentation mechanism at lower excitation energies near the onset of predissociation.[4,19–24] Okabe was the first who measured absorption and fluorescence excitation spectra of the $\tilde{C}\,^1B_2 \leftarrow \tilde{X}\,^1A_1$-system of gas-phase SO_2 at room temperature in the wavelength region 200–235 nm[19]. He attributed the sudden decrease of the fluorescence yield observed near 219 nm to the onset of predissociation. Later, fluorescence lifetime and absolute fluorescence quantum yield measurements from single vibronic states in the 210–230 nm absorption region of room-temperature SO_2 were performed by Hui and Rice.[20] In these studies a sharp drop in fluorescence lifetime and quantum yield was observed for wavelengths shorter than 220·6 nm. The results of subsequent predissociation threshold measurements by Ebata *et al*,[21] Kanamori *et al*,[14] and Ivanco *et al*[22] are discussed in detail by Becker *et al*[23,24] who investigated the dissociation of supersonic jet cooled SO_2 from selected single rovibrational levels of the $\tilde{C}\,^1B_2$ state. In these experiments the use of resonant enhanced multiphoton ionization (REMPI) TOF product detection allowed the measurement of all electronic and rovibrational quantum numbers of the O and SO fragments respectively, at

excitation energies near the $SO_2(\tilde{C}\ ^1B_2) \rightarrow SO(X^3\Sigma^-;\ v'' = 0) + O(^3P_{j=2})$ predissociation threshold [23]. Despite a large number of studies on the product-state resolved dissociation dynamics, to the best of our knowledge, no absolute product yields have been reported so far. In the present work, we measured the absolute quantum yield for $O(^3P)$ product formation after photoexcitation at the KrCl excimer laser wavelength (222·4 nm). The use of this wavelength allows selective excitation of the (1, 2, 2) vibronic band of the $SO_2(\tilde{C}\ ^1B_2)$ state, where the three numbers in parentheses, (n'_1, n'_2, n'_3), represent the vibrational quantum numbers of the symmetric stretch, the bend, and the anti-symmetric stretch normal-modes, respectively.[8] Our investigations are therefore complementary to the studies of Hui and Rice who determined absolute fluorescence quantum yields, Φ_f, by calibrating their relative measurements against the known fluorescence quantum yield of benzene.[20]

2. Experimental

Photodissociation studies were carried out in a flow reactor employing a pulsed laser pump-probe setup which was recently modified to allow VUV-LIF detection of $O(^3P)$ atoms.[25] A detailed description of the experimental setup has been given elsewhere.[26] Hence, only a brief summary of the experimental method will be given in the following.

SO₂ (Messer Griesheim, purity > 99·98%) was pumped through the flow reactor at room temperature. The SO₂ pressure in the cell was typically 30–55 mTorr (monitored by an MKS Baratron gauge). For photolytic calibration measurements, NO₂ (Messer Griesheim, purity > 99·98%) was passed through the cell at pressures of typically 10–30 mTorr. Gas flows were maintained at high enough rates to ensure gas renewal between successive laser shots at a laser repetition rate of 6 Hz.

An excimer laser (Lambda Physik EMG 102 MSC) operating at the KrCl emission wavelength (222·4 nm [27]) optimised for broadband operation with a spectral bandwidth of $80\ cm^{-1}$ (~0·4 nm)[28] and a pulse duration of 15–20 ns was used to photodissociate the SO₂ as well as the NO₂ molecules (used in the calibration measurements). Pump laser intensities were in the range 1–3 mJ/cm². Photolysis studies of SO₂ at 193·3 nm were performed with a Lambda Physik LPX 205 ArF excimer laser with a spectral bandwidth of $190\ cm^{-1}$ (~0·7 nm) at laser intensities of typically 0·5–1 mJ/cm² and 2 mTorr SO₂ pressure.

For VUV-LIF detection of $O(^3P_j)$ atoms via the three allowed $O(3s\ ^3S^\circ \leftarrow 2p\ ^3P_j)$ transitions,[29] narrow-band (bandwidth ~0·45 cm^{-1}) pulsed probe laser radiation (pulse duration 10–15 ns), tuneable in the wavelength region 130·2–130·7 nm was generated by sum-difference frequency conversion of dye laser radiation in Krypton. The generated VUV laser beam was separated from the unconverted laser radiation and aligned to overlap the pump beam at right angles in the viewing region of a LIF detector. The delay time between the pump and probe pulses was typically 250 ns, to allow collision-free detection of the nascent $O(^3P_j)$ fragments. Under these experimental conditions fly-out of $O(^3P)$ atoms, intramultiplet relaxation of the spin-orbit excited states $O(^3P_{j=1,0})$ by quenching and secondary reactions with SO₂ and NO₂, respectively, were negligible.

LIF was observed via a solar blind photomultiplier (THORN EMI model 9413 B) positioned at right angles to both pump and probe laser beams. The VUV probe beam intensity was monitored after passing through the reaction cell by an additional photomultiplier. For the subtraction of 'background' $O(^3P_j)$ atom signal generated by VUV

probe beam photolysis an electronically controlled mechanical shutter was inserted into the photolysis beam path, such that at each point of the $O(^3P_{j=2,1,0})$ spectra, the signal could first be averaged 30 times with the shutter opened and again averaged 30 times with the shutter closed. Finally, a point-by-point subtraction procedure was adopted, to obtain directly and on-line a LIF signal representing the contribution from $O(^3P_{j=2,1,0})$ atoms generated solely by the pump laser pulse. VUV probe and pump laser intensities were monitored and the LIF signal was normalised to both laser intensities. In the experiments care was taken that the $O(^3P_j)$ atom signals showed a linear dependence on the pump laser intensity. Figure 1 depicts results of such a linearity check which clearly confirms that the detected products originate from a one-photon dissociation process.

Experiments were also performed to measure the quantum yield of $O(^1D)$ in the photo-dissociation of NO_2 by making use of the fast reaction $O(^1D) + H_2 \rightarrow OH + H$. The nascent H atoms produced from the reaction were detected by the VUV-LIF using the Lyman a ·6 nm. For this purpose, narrow band VUV laser light tunable around the H atom Lyman α transition was generated by resonant third-order sum–difference frequency conversion of pulsed dye laser radiation in a phase-matched Kr–Ar mixture.[26] In the Kr four-wave mixing scheme ($w_{UV} = 2 \times w_R - w_T$) via which the VUV radiation was generated, the laser radiation of $I_R = 212·55$ nm is two-photon resonant with the Kr $(4p–5p)$ $[1/2, 0]$ transition and held fixed during the experiments, while w_T could be tuned from 844 to 846 nm to generate the VUV laser radiation covering the H atom Lyman–a transition. The fundamental laser radiation was obtained from two dye lasers simultaneously pumped by a XeCl excimer laser. In the first dye laser, coumarin 120 was used to generate the 425·1 nm radiation which was subsequently frequency doubled in a BBO crystal in order to obtain $I_R = 212·55$ nm. $I_T = 844–846$ nm was obtained by operating the second laser with Styryl 9 dye. The generated Lyman-a was carefully separated from the fundamental laser light by a lens monochromator followed by a light baffle system. A bandwidth of $\Delta w_{UV} \approx 0·4$ cm^{-1} was determined for the Lyman-a laser radiation in separate experiments by measuring H-atom Doppler profiles under thermalised conditions.
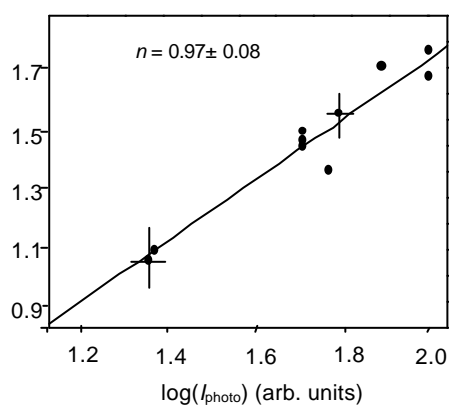

Figure 1.   Dependence of the observed $O(^3P_{j=2})$ atom LIF signal from SO_2 photolysis on the (222·4 nm) photolysis laser intensity (I_{photo}). The slope n of the fitted linear log–log plot is given in the figure.

3. Results

3.1 *O(^{3}P) fine-structure state distribution*

Figure 2 shows typical Doppler profiles of O(^{3}P$_{j=2,1,0}$) atoms produced in the gas-phase dissociation of SO$_2$ at room-temperature after excitation at 222·4 nm. The fine-structure state distribution of the O(^{3}P$_{j=2,1,0}$) fragments was determined from the integrated areas of the Doppler profiles after correcting for the slightly different oscillator strengths of the spectral transitions used in probing the different *j*-states.[29] Fine-structure state distributions were repeatedly measured at pump-probe delay times between 100 and 350 ns and at different SO$_2$ pressures in the range 30–55 mTorr. No significant differences in the distributions were observed under these experimental conditions. An evaluation of 40 Doppler profiles yielded the nascent population distribution $n_{j=2}/n_{j=1}/n_{j=0} = (0.88 \pm 0.02)/(0.10 \pm 0.01)/(0.02 \pm 0.01)$ for $j = 2$ (ground state), $j = 1$ (158·26 cm^{-1}) and $j = 0$ (226·98 cm^{-1}) where the errors represent the 1s statistical uncertainties of the experimental data. This distribution deviates significantly from the $n_{j=2}/n_{j=1}/n_{j=0} = (0.592 \pm 0.05)/(0.295 \pm 0.032)/(0.114 \pm 0.033)$ distribution reported for the 193·3 nm laser photolysis of SO$_2$ in ref. [17]. The latter is close to a statistical 'prior' distribution, $n_{j=2}/n_{j=1}/n_{j=0} = 0.56/0.33/0.11$, which is determined (in the limit of large excess energies) by the ratios of the $(2j + 1)$-degeneracies of the O(^{3}P$_j$) fine-structure states.[30] However, in view of the discrepancy between the O(^{3}P$_{j=2,1,0}$) fine-structure state distributions obtained in refs. [17, 18] after 193·3 nm excitation of SO$_2$ we also remeasured the O(^{3}P$_{j=2,1,0}$) fine-structure state distribution at that particular photolysis wavelength and obtained a clearly non-statistical distribution, $n_{j=2}/n_{j=1}/n_{j=0} = (0.70 \pm 0.01)/(0.21 \pm 0.01)/(0.09 \pm 0.01)$, which is (within the combined error bars) in very good agreement with the distribution obtained by Kawasaki and co-workers.[18]

3.2 *Absolute O(^{3}P) atom product quantum yield in the 222·4 nm photolysis of SO$_2$*

After having measured the O(^{3}P$_j$) distribution, the absolute primary product quantum yield, $\Phi_{O(^3P)}$, for O(^{3}P) formation in the 222·4 nm photolysis of SO$_2$ was obtained by
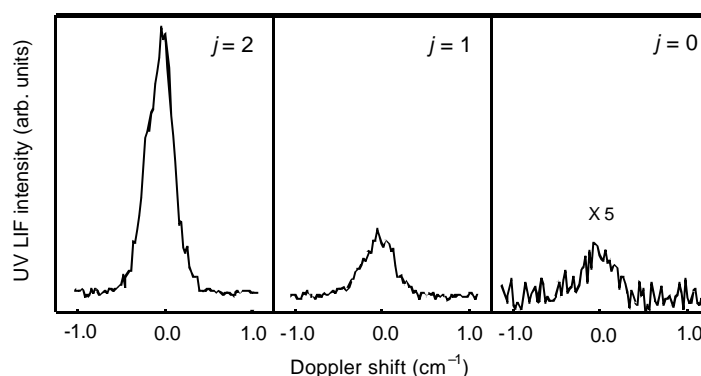

Figure 2. Vacuum ultraviolet LIF spectra of the O(^{3}P$_{j=2,1,0}$) atom products recorded 250 ns after pulsed (222·4 nm) excimer laser photolysis of 50 mTorr of SO$_2$. Line centers correspond to the ($3s\ ^3$S° $\leftarrow 2p\ ^3$P$_j$)-transition of the O(^{3}P$_{j=2}$), O(^{3}P$_{j=1}$) and O(^{3}P$_{j=0}$) atom fragments at 76794·98 cm^{-1}, 76636·72 cm^{-1} and 76568·00 cm^{-1} respectively.

calibrating the $O(^3P_{j=2})$ signal, $S_{j=2}(SO_2)$, measured in the SO_2 photodissociation against the $O(^3P_{j=2})$ signal, $S_{j=2}(NO_2)$, observed in the NO_2 photolysis at the same wavelength (see figure 3). Because the photolysis experiments were carried out under optically thin conditions – with only a few percent of the parent molecules being dissociated – and at identical photolysis laser intensities, the following relationship could be used in the evaluation of $\Phi_{O(^3P)}$:

$$\Phi_{O(^3P)} = \{S_{j=2}(SO_2)f_{O(^3P)}(NO_2)N_{j=2}(NO_2)\sigma_{NO_2}p_{NO_2}\}/$$
$$\{S_{j=2}(NO_2)n_{j=2}(SO_2)\sigma_{SO_2}p_{SO_2}\}, \tag{1}$$

where σ_{NO_2} and σ_{SO_2} are the room-temperature absorption cross-sections of NO_2 and SO_2 at 222·4 nm and p_{NO_2} and p_{SO_2} are the NO_2 and SO_2 pressures, respectively. The absorption cross sections $\sigma_{NO_2} = (4·2 \pm 0·2) \times 10^{-19}$ cm^2 and $\sigma_{SO_2} = (1·1 \pm 0·2) \times 10^{-18}$ cm^2 were obtained from the data given in ref. [31] respectively, taking into account the actual
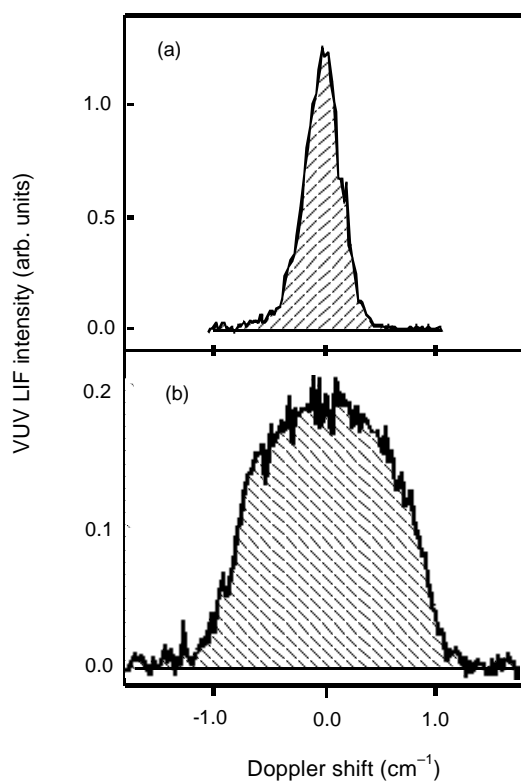
Figure 3. Comparison of Doppler profiles of $O(^3P_{j=2})$ atoms produced in the KrCl (222·4 nm) excimer laser photolysis of (**a**) 50 mTorr of SO_2 and (**b**) 29 mTorr of NO_2. Spectra were recorded 250 ns after the photolysis laser pulse. Line centers correspond to the $(3s\ ^3S° \leftarrow 2p\ ^3P_j)$-transition of the $O(^3P_{j=2})$ atoms (76794·98 cm^{-1}). Details about the photolytic calibration procedure for the measurement of the absolute $O(^3P)$ atom quantum yield are given in the text.

photolysis laser bandwidth. N$_{j=2}$(NO$_2$) and $n_{j=2}$(SO$_2$) are the relative populations of the respective O(^{3}P$_{j=2}$) states. The value $n_{j=2}$(SO$_2$) = (0·88 ± 0·02) could be taken from the measured fine-structure distribution given above. The UV photodissociation dynamics of NO$_2$ has been investigated in great detail (see, for example refs. [32–35], and references therein) but the nascent O(^{3}P$_j$) fine-structure distribution for the 222·4 nm photolysis wavelength has not been reported so far. It was therefore measured in the present study and the following result, $N_{j=2}/N_{j=1}/N_{j=0}$(NO$_2$) = (0·52 ± 0·03)/(0·33 ± 0·01)/(0·15 ± 0·02), was obtained, which is in good agreement with the O(^{3}P$_j$) fine-structure distribution obtained by Zare and co-workers for the 226 nm photolysis wavelength.[34]

The product branching into N + O$_2$, and O(^{1}D) + NO in the 228·8 nm photolysis of NO$_2$ was studied by Preston and Cvetanovic.[36] They demonstrated that N atom formation is unimportant and reported a value of 0·4 for the primary O(^{1}D) quantum yield. Later on, Uselman and Lee[37] measured O(^{1}D) quantum yields in the NO$_2$ photodissociation at different wavelengths in the region 248 to 213·9 nm. From their results, a value of $f_{O(^1D)}$(NO$_2$) = 0·44 for the 222·4 nm wavelength can be obtained using the best fit to the data points. With this value the quantum yield for O(^{3}P) formation could be calculated to be $f_{O(^3P)}$(NO$_2$) = 1−$f_{O(^1D)}$(NO$_2$) = 0·56. However, it is desirable to have an independent experimentally measured quantum yield value for O(^{1}D) at this wavelength. We used two different approaches for this purpose which are described below. In the first approach, the O(^{1}D) quantum yield of NO$_2$ was measured making use of the fast reaction O(^{1}D) + H$_2$ → H + OH, we observed the time evolution of the H atom products via LIF at the H atom Lyman-*a* wavelength (121·6 nm). Figure 4 shows the temporal evolution of H atoms produced in the reaction O(^{1}D) + H$_2$ → H + OH followed by the decay due to the H + NO$_2$ → OH + NO reaction. The production and decay of H atoms as a function of
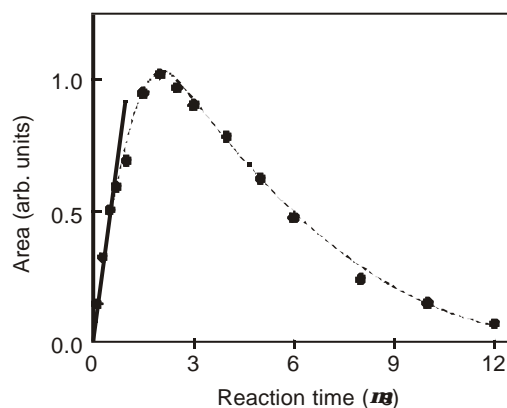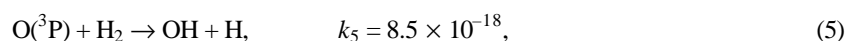

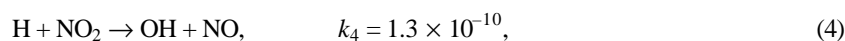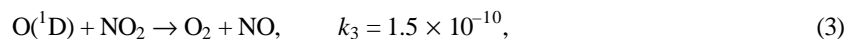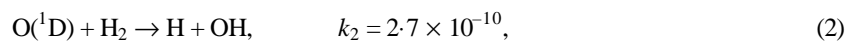**Figure 4.** Temporal rise and decay of H atoms formed in the reaction of O(^{1}D) atoms with H$_2$. O(^{1}D) atoms were produced by 222·4 nm photolysis of NO$_2$ in the presence of H$_2$ and He. (NO$_2$ pressure 31 mTorr, H$_2$ pressure 50 mTorr and rest He, total pressure 950 mTorr). H atoms were monitored via laser induced fluorescence (LIF) at the Lyman-*a* wavelength (121·6 nm). Straight line passing through the first three points indicates the region where linear approximation for the evaluation of the O(^{1}D) quantum yield in the 222·4 photolysis of NO$_2$ was used (see text for details). The dashed line shows the modelling of the curve using known rate constants from NIST data base.

time was modelled taking into account the following reactions and rate constants (given in units of cm^3 molecule^{-1} s^{-1}):

$$O(^1D) + H_2 \rightarrow H + OH, \qquad k_2 = 2.7 \times 10^{-10}, \tag{2}$$

$$O(^1D) + NO_2 \rightarrow O_2 + NO, \qquad k_3 = 1.5 \times 10^{-10}, \tag{3}$$

$$H + NO_2 \rightarrow OH + NO, \qquad k_4 = 1.3 \times 10^{-10}, \tag{4}$$

$$O(^3P) + H_2 \rightarrow OH + H, \qquad k_5 = 8.5 \times 10^{-18}, \tag{5}$$

$$O(^3P) + NO_2 \rightarrow O_2 + NO. \qquad k_6 = 9.7 \times 10^{-12}. \tag{6}$$
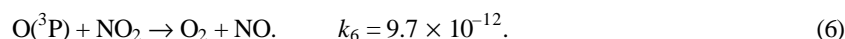
It must be noted here that the reaction of translationally hot O(^3P) atoms with H$_2$ can also produce H atoms. With rate constants for the reactions taken from ref. [38] and the pressures of different reactants, the dashed curve in figure 4 was obtained. For determination of the O(^1D) quantum yield, a more simplified approach was used. The left part of the curve (small delay times up to 500 ns) can be approximated by a linear curve. In this region, the increase of H atom concentration is only dependent on the delay time assuming $[H_2]_{(t)} \approx [H_2]_{(t=0)}$ and $[O(^1D)]_{(t)} \approx [O(^1D)]_{(t=0)}$. The absolute quantum yield can be derived from the integrated area of the Doppler profile by a photolytic calibration approach employing H$_2$S photolysis at 222·4 nm as a reference.[39] Figure 5a shows a H atom Doppler profile from the O(^1D) + H$_2 \rightarrow$ H + OH reaction measured at a delay time of 300 ns. A 'calibration H atom Doppler profile' obtained in the 222·4 nm photolysis of H$_2$S is shown in figure 5b. The following equation was used to calculate the absolute quantum yield of O(^1D):

$$f_{O(^1D)}(NO_2) = \{S_H(\text{reaction})s_{H_2S}[H_2S]\Phi_H(H_2S)\}/$$
$$\{S_H(H_2S\text{-calibration})s_{NO_2}[NO_2][H_2]k_2t\}, \tag{7}$$

where S_H denotes the integrated area of the respective H atom Doppler profile, s_{H_2S} and s_{NO_2} are the optical absorption cross section of H$_2$S and NO$_2$ at the 222·4 nm photolysis wavelength, k_2 is the rate constant for H atom production by the reaction of O(^1D) with H$_2$, t is the pump-probe delay time at which the H atom products were detected, [H$_2$S], [NO$_2$], and [H$_2$] are the concentrations of H$_2$S, NO$_2$, and H$_2$. The ratio of the optical absorption cross-sections s_{H_2S}/s_{NO_2} at 222·4 nm was determined in independent measurements to be 1·96 ± 0·20. The H atom quantum yield in the H$_2$S photolysis at 222·4 nm is unity: $\Phi_H(H_2S) = 1$. The rate constant k_2 for reaction of translationally excited O(^1D) atoms with H$_2$ which produces H atoms was studied earlier and the value of $k_2 = (2.7 \pm 0.6) \times 10^{-10}$ cm^3/s was determined.[40] Using this method, evaluation of the first three data points in figure 4 (up to $t = 500$ ns) yields an absolute quantum yield of $f_{O(^1D)}(NO_2) = 0.45 \pm 0.06$. The quoted error was calculated applying simple error propagation.

From measurements of O(^3P) Doppler profiles from the photolysis of NO$_2$ at 222·4 nm a translational temperature of ~3000 K could be derived. The rate constant for the reaction of O(^3P) with H$_2$ for this temperature is 10 times less than the one for O(^1D) reaction.[38] Correcting the above calculations with this value, a O(^1D) quantum yield for NO$_2$ is derived which is only marginally smaller than the one given above. It is therefore assumed that the reaction of O(^3P) can be neglected and in the further discussion a O(^1D) quantum yield of $f_{O(^1D)}(NO_2) = 0.45 \pm 0.06$ will be used.
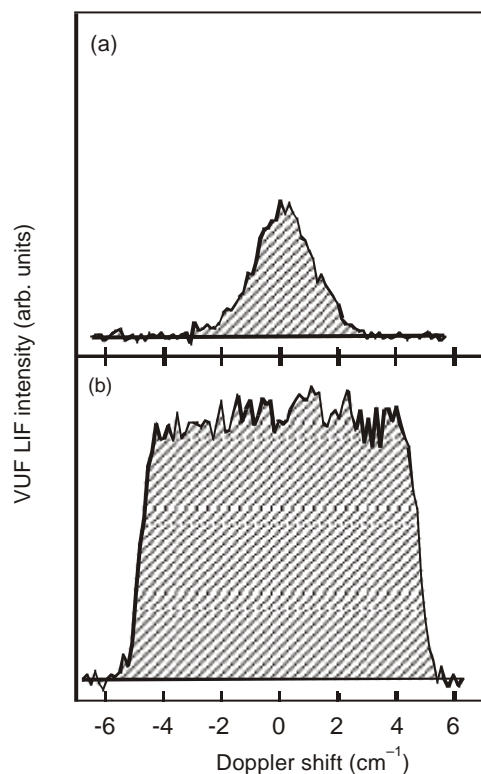
Figure 5. (**a**) Doppler profile of H atoms produced in the O(^{1}D) + H$_2$ reaction measured after 300 ns (experimental conditions as in figure 4). (**b**) H atom Doppler profile measured in the 222·4 nm photolysis of H$_2$S (calibration) under collision-free conditions (H$_2$S pressure 4 mTorr, pump-probe delay time 100 ns). The centers of the Doppler profiles correspond to the ($2p^2$P $\leftarrow$ $1s^2$S) Lyman-*a* transition of the H atom (82259 cm^{-1}).

In addition to the method described above, we carried out another set of independent measurements in which the 222·4 nm photolysis of NO$_2$ (4 mTorr) was performed in the presence of a large excess of N$_2$ (860 mTorr) to determine the time dependent increase of the initial O(^{3}P) concentration due to additional O(^{3}P) atoms formed by the quenching process of the O(^{1}D) fragments by N$_2$. It should be noted that monitoring the relative rise in a given j level of O(^{3}P) could give erroneous results due to the inter relaxation of different j levels. Hence in the present work, the temporal profiles of O(^{3}P$_{j=2,1,0}$) were taken individually under similar experimental conditions and summed up, after due correction of oscillator strength, to get the overall temporal profile of O(^{3}P) up to 15 μs. In these studies the O(^{3}P) quantum yield, $f_{O(^3P)}$(NO$_2$) = [O(^{3}P)]/[O(^{3}P) + O(^{1}D)], can be directly obtained by comparing the O(^{3}P) concentrations measured right after the photolysis pulse with the O(^{3}P) concentrations at delay times of ~15 **m** at which all the O(^{1}D) atoms produced in the NO$_2$ photolysis are quenched to O(^{3}P) atoms. The quantum yield of O(^{1}D) obtained in this way was comparable to that obtained by the O(^{1}D) + H$_2$

reaction method. The results of these two measurement, $f_{O(^1D)}(NO_2) = 0.45 \pm 0.06$, are in good agreement with the value of 0·44 obtained by fitting the results of Uselmann and Lee.[37] Since N atom formation has been shown to be unimportant,[36] the quantum yield of O(^{3}P) in the 222·4 nm photolysis of NO$_2$ is $f_{O(^3P)}(NO_2) = 1 - f_{O(^1P)}(NO_2) = 0.55$. The latter value was used in the present evaluation of the O(^{3}P) quantum yield in the 222·4 nm photolysis of SO$_2$ via (1), which resulted in an average value of $\Phi_{O(^3P)} = 0.13 \pm 0.05$. The quoted experimental error was calculated from the errors of the entries of (1) on the basis of simple error propagation.

4. Discussion and conclusion

The absolute O(^{3}P) quantum yield $\Phi_{O(^3P)} = 0.13 \pm 0.05$ of the present work can directly be compared with the result of the absolute fluorescence quantum yield measurements carried out by Hui and Rice for SO$_2$ at room-temperature under bulb conditions.[20] In the latter work, for the 222·4 nm wavelength which leads to a selective excitation of the highly structured $\tilde{C}\,^1B_2(1, 2, 2) \leftarrow \tilde{X}\,^1A_1(0, 0, 0)$ vibronic band of SO$_2$ a value of $\Phi_f = 0.845 \pm 0.127$ was derived. This value is in very good agreement with the O(^{3}P) quantum yield obtained in the present study. Both results clearly demonstrate that appreciable amounts of O(^{3}P) atoms are produced after photoexcitation of SO$_2$ at room-temperature at 222·4 nm. However, because the energy of a 222·4 nm laser photon (44964 cm^{-1}) is lower than the SO$_2(\tilde{C}\,^1B_2) \rightarrow$ SO$(X^3\Sigma^-; v'' = 0) + $O($^3P_{j=2}$) dissociation threshold energy of $D_0 = 45725.3(1)$ cm^{-1} determined in ref. [23] only those SO$_2$ ground-state parent molecules with a rotational energy, E_{rot}, higher than $D_0 - \hbar w_{pump} \approx 761$ cm^{-1} can actually be dissociated. Using the SO$_2(\tilde{X}\,^1A_1)$ ground-state molecular constants given in ref. [41] the fraction of room-temperature SO$_2$ molecules with $E_{rot} > 761$ cm^{-1} can be estimated to be about 0·17.[42] Comparison of this value with the O(^{3}P) quantum yield measured in the present study shows that about 75% of the SO$_2$ parent molecules with $E_{rot} > 761$ cm^{-1} contribute to O(^{3}P) atom formation suggesting that the initial SO$_2$ rotational excitation plays an important role in the dissociation of the $\tilde{C}\,^1B_2(1, 2, 2)$ vibronic level. The rovibrational dependence of the predissociation rate in the $\tilde{C}\,^1B_2$ state of SO$_2$ was investigated by Ebata *et al.*[21] In their LIF studies of SO$_2$ at room-temperature they observed that for vibronic bands located at excitation energies higher than 45400 cm^{-1} the fluorescence lifetime of the bandheads (occurring at low rotational numbers) is significantly longer than that of the higher rotational levels (see table 2 of ref. [21]) indicating that high rotational levels are more predissociative than low levels. However, their final conclusion that predissociation occurs by curve crossing with the repulsive triplet state has to be questioned in the light of the recent results obtained by Becker *et al*,[22] who demonstrated that predissociation is caused by coupling to a bound potential surface which correlates with SO($X^3\Sigma^-$) and O(^{3}P) products without a reaction barrier. The latter result is in agreement with the results reported in refs. [8, 14, 32] which clearly showed that photodissociation via the $\tilde{C}\,^1B_2$ state proceeds mainly through vibronic mixing between the $\tilde{C}\,^1B_2$ state vibronic levels and the quasi-bound dissociation continuum of the $\tilde{X}\,^1A_1$ ground-state. Hence it can be concluded that the O(^{3}P) formation observed in the present study for SO$_2$ at room-temperature is due to a similar mechanism in which the predissociation occurs, however, to a large extent via high rotational states of the optically prepared $\tilde{C}\,^1B_2 (1, 2, 2)$ vibronic level.

Acknowledgments

References

1. Georgii H W and Warneck P 1999 in *Global aspects of atmospheric chemistry* (ed.) R Zellner (Springer: Berlin), and references therein
2. Ploch H J and Troe J 1984 *J. Chem. Kinet.* **16** 1531, and references therein
3. Jackson W M and Okabe H 1986 *Advan. Photochem.* **13** 17
4. Okabe H 1978 *The photochemistry of small molecules* (New York: Wiley)
5. Dastageer A, Hegazi E, Hamadan A and Al-Adel F 1999 *J. Chem. Phys.* **111** 1784
6. Ray P C, Arendt M F and Butler L J 1998 *J. Chem. Phys.* **109** 5221, and references therein
7. Brand J C D, Chiu P H, Hoy A R and Bist H D 1976 *J. Mol. Spectros.* **60** 43
8. Katagiri H, Sako T, Hishikawa A, Yazaki T, Onda K, Yamanouchi K and Yoshino K 1997 *J. Mol. Struct.* **413** 589, and references therein
9. Freedman A, Yang S C and Bersohn R 1979 *J. Chem. Phys.* **70** 5313
10. Kawasaki M, Kasatani K, Sato H, Shinoha H and Nishi N 1982 *Chem. Phys.* **73** 377
11. Kawasaki M and Sato H 1987 *Chem. Phys. Lett.* **139** 585
12. Felder P, Effenhauser C S, Haas B M and Huber J R 1988 *Chem. Phys. Lett.* **148** 417
13. Felder P, Hass B-M and Huber J R 1993 *Chem. Phys. Lett.* **204** 248
14. Kanamori H, Butler J E, Kawaguchi K, Yamada C and Hirota E 1985 *J. Chem. Phys.* **83** 611
15. Chen X, Asmar F, Wang H and Weiner B R 1991 *J. Phys. Chem.* **95** 6415
16. Hansen N, Andresen U, Dreizler H, Grabow J U, Mader H and Temps F 1998 *Chem. Phys. Lett.* **289** 311
17. Huang Y-L and Gordon R J 1990 *J. Chem. Phys.* **93** 868
18. Abe M, Sato Y, Inagaki Y, Matsumi Y and Kawasaki M 1994 *J. Chem. Phys.* **101** 5647
19. Okabe H 1971 *J. Am. Chem. Soc.* **93** 7095
20. Hui M-H and Rice S A 1972 *Chem. Phys. Lett.* **17** 474
21. Ebata T, Nakazawa O and Ito M 1988 *Chem. Phys. Lett.* **143** 31
22. Ivanco M, Hager J, Sharfin W and Wallace S C 1983 *J. Chem. Phys.* **78** 6531
23. Becker S, Braatz C, Linder J and Tiemann E 1995 *Chem. Phys.* **196** 275
24. Braatz C and Tiemann E 1998 *Chem. Phys.* **229** 93
25. Ebert V, Schulz C, Volpp H-R, Wolfrum J and Monkhouse P 1999 *Isr. J. Chem.* **39** 1
26. Brownsword R A, Hillenkamp M, Laurent T, Vatsa R K and Volpp H-R 1997 *J. Chem. Phys.* **106** 4436
27. Armandillio E, Luches A, Nassisi V and Perrone M R 1985 *Appl. Opt.* **24** 18
28. Decker M and Sick V 1996 *Appl. Opt.* **35** 482
29. Radzig A A and Smirnov B M 1985 *Reference data on atoms, molecules and ions* (Springer: Heidelberg)
30. Levine R D and Bernstein R B 1987 *Molecular reaction dynamics and chemical reactivity* (Oxford: University Press)
31. (a) Röth E-P, Runke R, Moortgat G, Meller R and Schneider W *UV/VIS-Absorption cross sections and quantum yields for use in photochemistry and atmospheric modeling, Part 1: Inorganic substances*, Berichte des Forschungszentrums Jülich; Nr. 3340 (ISSN 0944-2952), Jülich, Germany; (b) Bass A M, Ledford A E and Lauffer A 1976 *J. Res. Natl. Bur. Stand.* **A80** 143

32. Troe J 1983 *J. Chem. Phys.* **79** 6017
33. Robra U, Zacharias H and Welge K H 1990 *Z. Phys. D.* **16** 175
34. Rubahn H G, van der Zande W J, Zhang R, Bronikowski M J and Zare R N 1991 *Chem. Phys. Lett.* **186** 154
35. Reid S A and Reisler H 1994 *J. Chem. Phys.* **101** 5683
36. Preston K F and Cvetanovic R J 1966 *J. Chem. Phys.* **45** 2888
37. Uselman W M and Lee E K C 1976 *J. Chem. Phys.* **65** 1948
38. DeMore W B, Sander S P, Golden D M., Hampson R F, Kurylo M J, Howard C J, Ravishankara A R, Kolb C E and Molina M J 1992 *Chemical kinetics and photochemical data for use in stratosphere modeling,* No. 10, NASA, JPL Publication 92–20. For reaction 3 the latest value reported by R F Curl *et al* (*Chem. Phys. Lett.* 337 (2001) 72) is $(1\cdot5 \pm 0\cdot3) \times 10^{-10}$ cm^3 molecule^{-1} s^{-1}
39. Brownsword R A, Hillenkamp M, Volpp H-R and Vatsa R K 1999 *Res. Chem. Intermed.* **25** 339
40. Koppe S, Laurent T, Naik P D, Volpp H-R, Wolfrum J, Arusi-Parpar T, Bar I and Rosenwaks S 1993 *Chem. Phys. Lett.* **214** 546
41. Herzberg G 1960 *Electronic spectra and electronic structure of polyatomic molecule* (Van Nostrand: Princeton)
42. For details, see chapter I-4.3. of ref. 4